

1 **A machine learning approach to produce a continuous solar-induced chlorophyll**  
2 **fluorescence dataset for understanding Ocean productivity**

3 Nima Madani<sup>1,2</sup>, Nicholas C. Parazoo<sup>2</sup>, Manfredi Manizza<sup>3</sup>, Abhishek Chatterjee<sup>2</sup>, Dustin  
4 Carroll<sup>4</sup>, Dimitris Menemenlis<sup>2</sup>, Vincent Le Fouest<sup>5</sup>, Atsushi Matsuoka<sup>6</sup>, Kelly M. Luis<sup>2</sup>, Camila  
5 Serra Pompei<sup>7</sup>, Charles E. Miller<sup>2</sup>

6 <sup>1</sup>UCLA Joint Institute for Regional Earth System Science and Engineering, 4242 Young Hall,  
7 607 Charles E. Young Drive East, Los Angeles, CA 90095, USA.

8 <sup>2</sup>Jet Propulsion Laboratory, California Institute of Technology, 4800 Oak Grove Drive, Pasadena, CA 91109, USA.

9 <sup>3</sup>University of California San Diego, Geosciences Research Division, Scripps Institution of Oceanography 500 Gilman Drive La  
10 Jolla, CA 92093, USA.

11 <sup>4</sup>Moss Landing Marine Laboratories, San José State University, Moss Landing, California, USA

12 <sup>5</sup>Littoral Environnement et Sociétés, UMR 7266, Université de La Rochelle, La Rochelle, France

13 <sup>6</sup>UNH Marine Science & Ocean Engineering, Morse Hall, Durham, NH 03824, USA

14 <sup>7</sup>Center for Climate Change Science, Massachusetts Institute of Technology, Cambridge, MA, USA

15 **Corresponding author:** Nima Madani, Email:[nima.madani@jpl.nasa.gov](mailto:nima.madani@jpl.nasa.gov)

16 **Abstract**

17 Phytoplankton primary production is a crucial component of Arctic Ocean (AO)  
18 biogeochemistry, playing a pivotal role in the carbon cycling by supporting higher trophic levels  
19 and removing atmospheric carbon dioxide. The advent of satellite observations measuring  
20 chlorophyll a concentration (Chl<sub>a</sub>) has yielded unprecedented insights into the distribution of  
21 AO phytoplankton, enhancing our ability to assess oceanic productivity. However, the optical  
22 properties of AO waters differ significantly from those of lower-latitude waters, and standard  
23 Chl<sub>a</sub> algorithms perform poorly in the AO. In particular, Chl<sub>a</sub> retrievals are challenged by  
24 interferences from other marine constituents including higher pigment packaging and higher  
25 proportion of light absorption by colored dissolved organic matter. To derive phytoplankton-  
26 originating signature as well as mitigate those effects, solar-induced chlorophyll fluorescence  
27 (SIF) emerges as a valuable tool for acquiring physiological insights into the direct  
28 photosynthetic processes in the AO. In this study, we leverage satellite-based SIF measurements  
29 to assess their correlation with a set of predictive factors influencing phytoplankton  
30 photosynthesis. We extend the temporal coverage of AO SIF data to cover the period 2004 -  
31 2020. This novel dataset offers a pathway to monitor the physiological interactions of  
32 phytoplankton with changes in climate, promising to significantly improve our understanding of  
33 the Arctic water's productivity. The application of this data is expected to provide insights into  
34 how phytoplankton respond to shifts in environmental changes, contributing to a more nuanced  
35 understanding of their role in High-Latitude Northern Oceans ecosystems.

36

37 **Key Points**

- 38 • We extrapolated red SIF over the period of 2004-2020 using a set of predictive variables  
39 influencing photosynthesis over the Arctic Ocean.  
40 • The reconstructed SIF data demonstrates a strong correlation with independent data  
41 records.

- Data produced is expected to provide a new insight into assessment of Arctic Ocean productivity.

44

45

## 46 **Plain Language Summary**

47 Phytoplankton communities, via means of photosynthesis, play a crucial role in the global carbon  
48 cycle by transforming carbon dioxide into organic matter. Recognizing the importance of ocean  
49 productivity is essential for effectively managing and conserving marine ecosystems, promoting  
50 sustainable fisheries, and comprehending the broader ramifications of climate change on the  
51 world's oceans. Alterations in ocean productivity, especially shifts in the abundance and  
52 composition of phytoplankton, can serve as early indicators of the health of aquatic ecosystems.  
53 While satellite observations have provided an unprecedented overview of phytoplankton  
54 distribution by estimating chlorophyll concentrations over oceans, uncertainties persist regarding  
55 the accurate estimation of the total photosynthetic activity of organisms in the ocean. Recently,  
56 the TROPOMI satellite instrument has made solar-induced chlorophyll fluorescence (SIF) data  
57 available, offering another metric for understanding photosynthetic activity. However, the short  
58 latency of the data record makes it challenging to assess the impact of rapid climate change in  
59 the Arctic domain. In this paper, we employ a modeling framework to extend SIF data over a  
60 more extended period, facilitating a more comprehensive assessment of ocean productivity.

## 61 **1- Introduction**

62 Increasing atmospheric growth rate of CO<sub>2</sub> represents a higher proportion of fossil fuel emission  
63 relative to natural compensation and negative feedback of terrestrial and aquatic ecosystems  
64 through photosynthesis. While global ocean productivity is estimated to be ~50–60 Pg yr<sup>-1</sup>  
65 (Johnson and Bif 2021, Buitenhuis *et al* 2013), oceans are responsible for an annual carbon sink  
66 of 2.9±0.4 Pg (Friedlingstein *et al* 2023). Oceanic primary productivity model estimates rely on  
67 satellite estimation of phytoplankton biomass (mg C m<sup>-3</sup>) and the phytoplankton growth rate (μ,  
68 d<sup>-1</sup>), integrated over the euphotic depth (Westberry *et al* 2008, Silsbe *et al* 2016, Behrenfeld and  
69 Falkowski 1997). Apart from limitation of the models, there are uncertainties arise from satellite  
70 observed reflectance band employed to retrieve chlorophyll-a (Chl\_a) concentration estimates  
71 that rely on empirical to semi-analytical relationships derived from the correlations between in-  
72 situ measurements and satellite reflectance bands in the blue-to-green region of the visible  
73 spectrum (Hu *et al* 2019, 2012, Li *et al* 2023). These algorithms have been implemented by  
74 multiple satellite instruments (e.g. CZCS; SeaWiFS and MODIS) since 1978 and have been used

75 to estimate photosynthetic rates from estimated chlorophyll concentration estimates (Behrenfeld  
76 and Falkowski 1997).

77 Rapid climate change is actively influencing the Arctic Ocean's unique ecosystem, resulting in  
78 rapid alterations in Chl<sub>a</sub> concentration and spatial distribution (Bouman *et al* 2020, Lewis *et al*  
79 2020). The retreat of sea- ice cover and subsequent changes in light availability and nutrient  
80 cycling have complex and sometimes opposing effects on chlorophyll levels (Dvoretzky *et al*  
81 2023, Castagno *et al* 2023). Warmer temperatures and melting sea ice have increased light  
82 availability and lengthened phytoplankton growing season, even promoting a second, late season  
83 bloom in some locations (Zhao *et al* 2022, Ardyna *et al* 2014, Manizza *et al* 2023). Changes in  
84 surface temperature, nutrient and light availability, salinity, wind stress, and increased freshwater  
85 input from melting ice and increased river runoff are among the factors that could affect  
86 phytoplankton photosynthesis and thus oceanic NPP (Ko *et al* 2022, Singh *et al* 2023).

87 Satellite measurements of Chl<sub>a</sub> provide a valuable and efficient tool for monitoring ocean  
88 chlorophyll content, spatial and temporal distribution patterns, and marine primary productivity.  
89 However, accuracy of ocean color algorithms is also impacted by high concentration of colored  
90 dissolved organic matter and pigment packaging effect in the AO which interferes with  
91 chlorophyll retrievals (Matsuoka *et al* 2017, Cota *et al* 2003). Additionally, the frequent presence  
92 of surface chlorophyll in the AO as well as a subsurface chlorophyll maximum (SCM) caused by  
93 sea ice melt can be a source of pixel contamination in the retrieval of satellite chlorophyll  
94 measurements, which potentially increases the uncertainty in primary productivity estimates  
95 (Bélanger *et al* 2007, Arrigo and Van Dijken 2011, Bouman *et al* 2020, Lee *et al* 2015).

96 Solar induced chlorophyll fluorescence (SIF) represents a promising alternative to quantify AO  
97 productivity without the spectroscopic challenges that hamper chlorophyll retrievals. The SIF  
98 signal represents 1-2% of photosynthetically active radiation re-emitted in red to near-infrared  
99 spectral range (Köhler *et al* 2020a, Parazoo *et al* 2019, Köhler *et al* 2018). SIF is closely related  
100 to terrestrial gross primary productivity (Frankenberg *et al* 2011, Guanter *et al* 2014, Parazoo *et*  
101 *al* 2014). The recent development of red SIF (Köhler *et al* 2020a) provides an unprecedented  
102 opportunity to quantify primary productivity from aquatic ecosystems. Red SIF is derived from  
103 Bands 5 and 6 of the TROPospheric Monitoring Instrument (TROPOMI), encompassing  
104 wavelengths of 661–725 nm and 725–775 nm, respectively. Red SIF generally correlates with

105 MODIS normalized fluorescence line height (nFLH, Behrenfeld et al 2009); however, notable  
106 differences are reported for specific regions (Köhler *et al* 2020a). In particular, nFLH retrievals  
107 face challenges in regions characterized by high chlorophyll concentrations (Gupana et al 2021);  
108 red SIF does not have this limitation.

109 Despite its advantages, the red SIF record only extends back to 2018, limiting its use in studying  
110 long-term change. We overcome this limitation by employing a randomForest (RF) machine  
111 learning model to provide continuous red SIF data spanning the period from 2004 to 2020. We  
112 compare our AO red SIF product to AO chlorophyll and NFLH products and discuss their  
113 similarities and differences. We conclude with observations on the potential for using red SIF to  
114 study marine PP trends in the rapidly evolving Arctic ecosystems.

115

## 116 **2- Methodology**

### 117 ***2.1 Datasets***

118 The TROPOMI sensor onboard the Sentinel-5 satellite provides wavelengths to capture SIF  
119 spectra for monitoring terrestrial and aquatic photosynthetic activity. Global retrievals of red  
120 wavelength SIF data have the advantage of retrieving photosynthetic information in variable  
121 atmospheric conditions with ~5km spatial resolution (Köhler *et al* 2020b). SIF signal is capable  
122 of penetrating through cloud and aerosol layer and unlike traditional usage of visible spectral  
123 bands, SIF is a photosynthesis by-product and insensitive to ocean color, which provides an  
124 unprecedented opportunity to monitor oceanic photosynthetic activity. Despite advantages of  
125 oceanic red SIF from TROPOMI, the recent availability of data (from Apr-2018) makes  
126 quantifying long-terms trends and anomalies in the aquatic systems challenging.

127 Recently, machine learning methods have been used to extrapolate and upscale SIF in terrestrial  
128 ecosystems using a combination of MODIS reflectance (e.g. CSIF; (Zhang *et al* 2018)) or  
129 reflectance and meteorological data (GOSIF; (Li and Xiao 2019)). These methods that are very  
130 common in remote sensing and ecosystem process analyses and predictions (Jung *et al* 2011,  
131 Madani *et al* 2018, Natali *et al* 2019), operate by predicting unavailable data using quantified  
132 relationships between observable and explanatory variables.

133 Here, we generate spatial and temporally coherent red-SIF products beyond the original retrieved  
 134 data that covers Apr 2018 to Apr 2021. In this approach, we first train monthly RF models using  
 135 the TROPOMI SIF climatological records over selected predictive variables that are believed to  
 136 impact quantic vegetation’s photosynthetic activity (Table 1). Subsequently, we predict SIF over  
 137 the 2004–2020 period using temporal information provided by each of the explanatory variables.

138 **Table 1. List of candidate explanatory variables for prediction of TROPOMI red-SIF over**  
 139 **the period of 2004-2020.**

Variable	Abbreviation	Spatial resolution	Source
Chlorophyll-a Concentration	Chl_a	Retrieved at 0.05°	(NASA 2014)
Normalized Fluorescence Line Height	nFLH*	Retrieved at 0.05o	(NASA 2014)
Sea Surface Temperature	SST*	Retrieved at 0.05°	(NASA 2014)
Sea Surface Salinity	SSS*	0.25 °	(Carroll <i>et al</i> 2020)
Meridional Wind Stress	vWind	0.25 °	(Carroll <i>et al</i> 2020)
Zonal Wind Stress	uWind*	0.25 °	(Carroll <i>et al</i> 2020)
Surface-ocean U Velocity	U	0.25 °	(Carroll <i>et al</i> 2020)
Surface-ocean V Velocity	V*	0.25 °	(Carroll <i>et al</i> 2020)
Distance from Coastal Zones	Distance*	0.05°	(Carroll <i>et al</i> 2020)
Aquatic Ecoregions	Ecoregions*	-	(Spalding <i>et al</i> 2007)

140 \* Next to the abbreviated variables indicates that they were used in the final model.

141 Explanatory variables were selected to represent spatial distribution of phytoplankton  
 142 communities as well as representing biotic, abiotic and physical characteristics of marine  
 143 ecosystems across the Arctic domain. We obtained MODIS Chl\_a and NFLH from Google Earth  
 144 Engine (Gorelick *et al* 2017), where we calculated monthly means based on 0.05 degree spatial  
 145 resolution, consistent with TROPOMI SIF data. Marine biophysical data obtained were from  
 146 ECCO-Darwin data assimilation model estimates (Carroll *et al* 2020). Aquatic ecoregions  
 147 (Spalding *et al* 2007) were used as a proxy to represent seasonal nutrient cycle and availability  
 148 across the Arctic ecosystems. Additionally, we calculated Euclidian distance from the coastal  
 149 zones to represent nutrient transport along the land-ocean continuum. All analysis were  
 150 performed in R (Core Team 2017) using open source libraries.

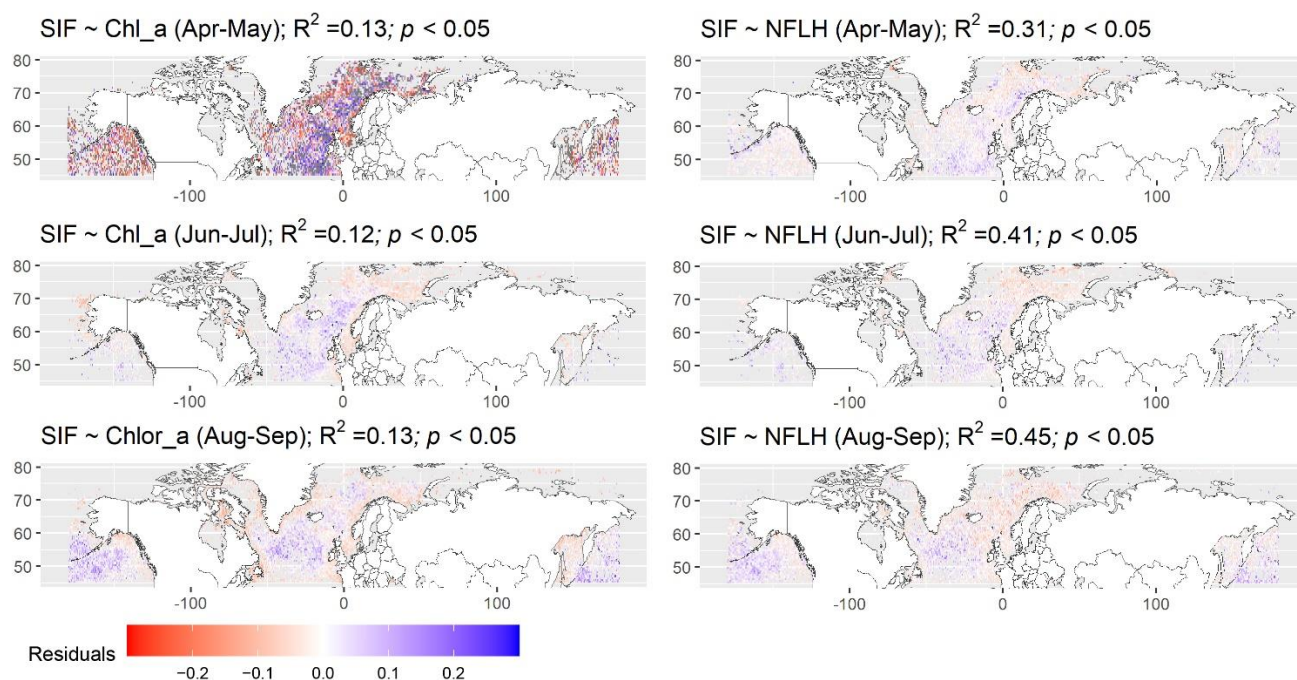
151            **2.2 Modeling and validation**

152 We developed a RF machine-learning model (Liaw and Wiener 2002) to examine the factors  
153 influencing the seasonal variation in SIF cross our 50-90° N study area (Figure 1). Our objective  
154 was to attribute the observed SIF patterns to potential underlying biotic and abiotic factors, as  
155 outlined in Table 1. For each month, we randomly sampled 70% of the data within the study area  
156 and linked it to corresponding information extracted from predictor variables.



157  
158 *Figure 1. Study domain indicating ocean bathymetry (in meters) and major regions.*

159 Decision Trees offer the advantage of capturing both linear and non-linear relationships between  
160 responses and target variables by categorizing data through a series of if-else nodes. At each  
161 terminal node, the mean value of observations within that region is calculated. We assessed the  
162 predictive power of MODIS Chlor\_a and NFLH as the main predictive component of the model  
163 (Figure 2). MODIS NFLH provided higher proportion of the variance in spatio-temporal  
164 correlations with the observed SIF over the study domain compared to Chl\_a.



165

166 *Figure 2. Spatial correlation between observed TROPOMI SIF (Solar-Induced Fluorescence)*  
167 *with MODIS Chlorophyll-a (Chl\_a) and Normalized Fluorescence Line Height (NFLH). Color*  
168 *palette indicates residuals of SIF values when linearly associated with Chl\_a and NFLH.*  
169 *Warmer and cooler colors indicate regions where SIF may be underestimated and overestimated*  
170 *when using Chl\_a and NFLH as linear predictors. A higher proportion of variance ( $R^2$ ) in SIF is*  
171 *explained by NFLH compared to Chl\_a.*

172

173 A stronger spatial correlation between the observed seasonality SIF relative to MODIS-derived  
174 NFLH and Chl\_a is also evident over temperate and polar ecoregions as well as selected regions  
175 (Figure S1, S2; supplementary materials). To prevent overfitting, we constrained the number of  
176 trees to reduce the RMSE of the prediction and maximize the performance of the model.  
177 Variable selection involved using a stepwise technique to identify a minimal set of variables  
178 adequate for robustly predicting the response variable (Genuer *et al* 2010).

179 We constructed RF models to evaluate the importance of explanatory variables in elucidating the  
180 heterogeneity in SIF trends throughout the seasons. These models quantify an increase in mean  
181 squared error (IncMSE) upon permuting each variable, indicating the significance of individual  
182 factors in explaining pixel-level heterogeneity relative to monthly SIF observations. Model

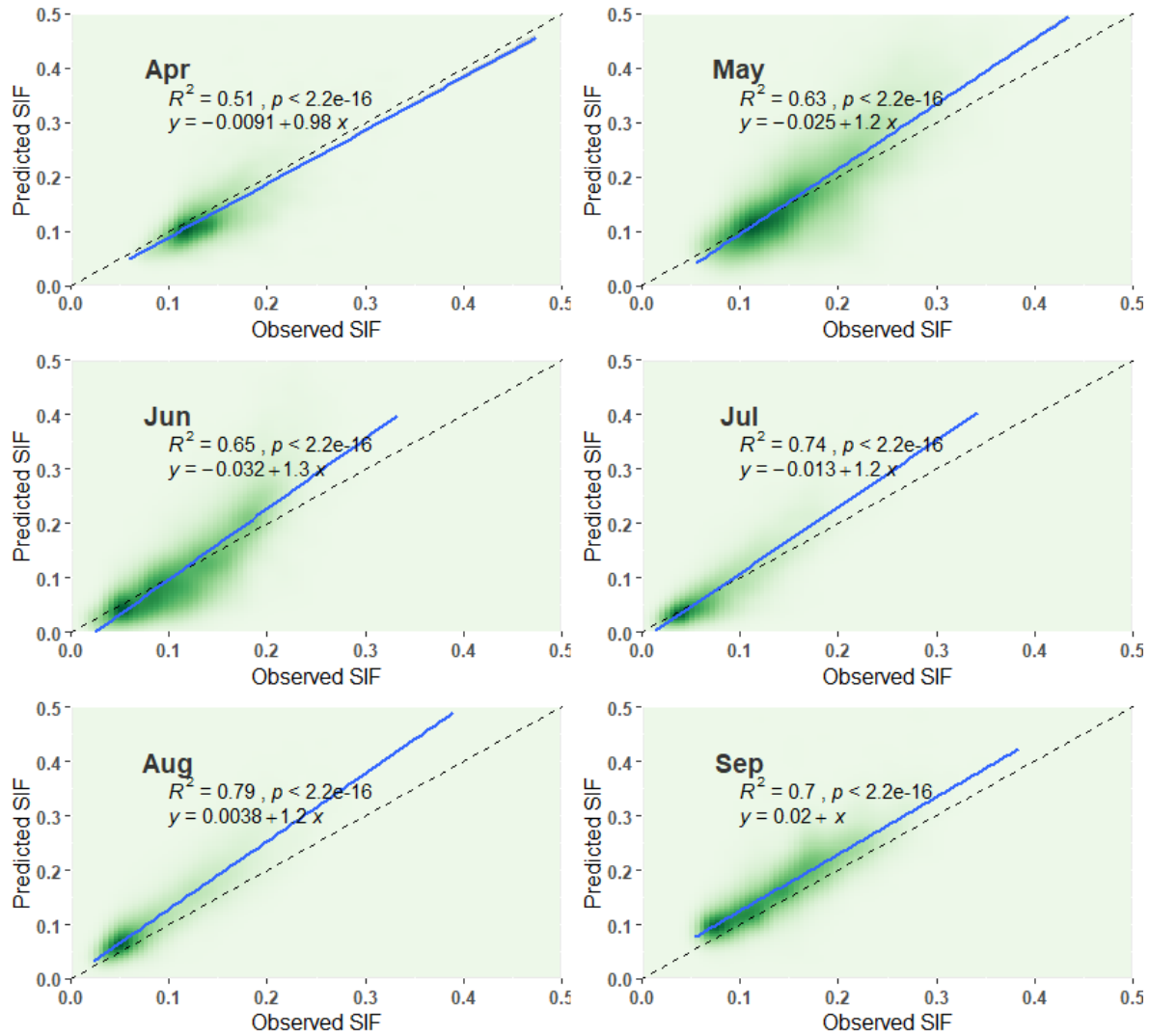
183 validation and testing were conducted on the remaining 30% of independent pixels. Additional  
184 analyses were performed at regional scales, and the predicted SIF data were compared with in-  
185 situ chlorophyll data obtained from the Tara Oceans Polar Circle 2013 cruises (Guidi *et al* 2017).

### 186 **3- Results and Discussion**

187 The RF model was used to assess the importance of each selected explanatory variable to predict  
188 SIF over the Arctic domain. Our model demonstrated an accuracy of 86% in elucidating spatial  
189 variability in SIF across independent testing data during the peak of the chlorophyll bloom.

190 Variables such as NFLH, SST, and SSS emerge as among the most important factors in  
191 explaining SIF spatial variability (Fig S3). Both SST and SSS served as indicators for spatial  
192 variations in optimal environmental conditions for phytoplankton photochemical processes.

193 When used in conjunction with NFLH as a proxy for fluorescence reflectance, they improved  
194 SIF prediction significantly.

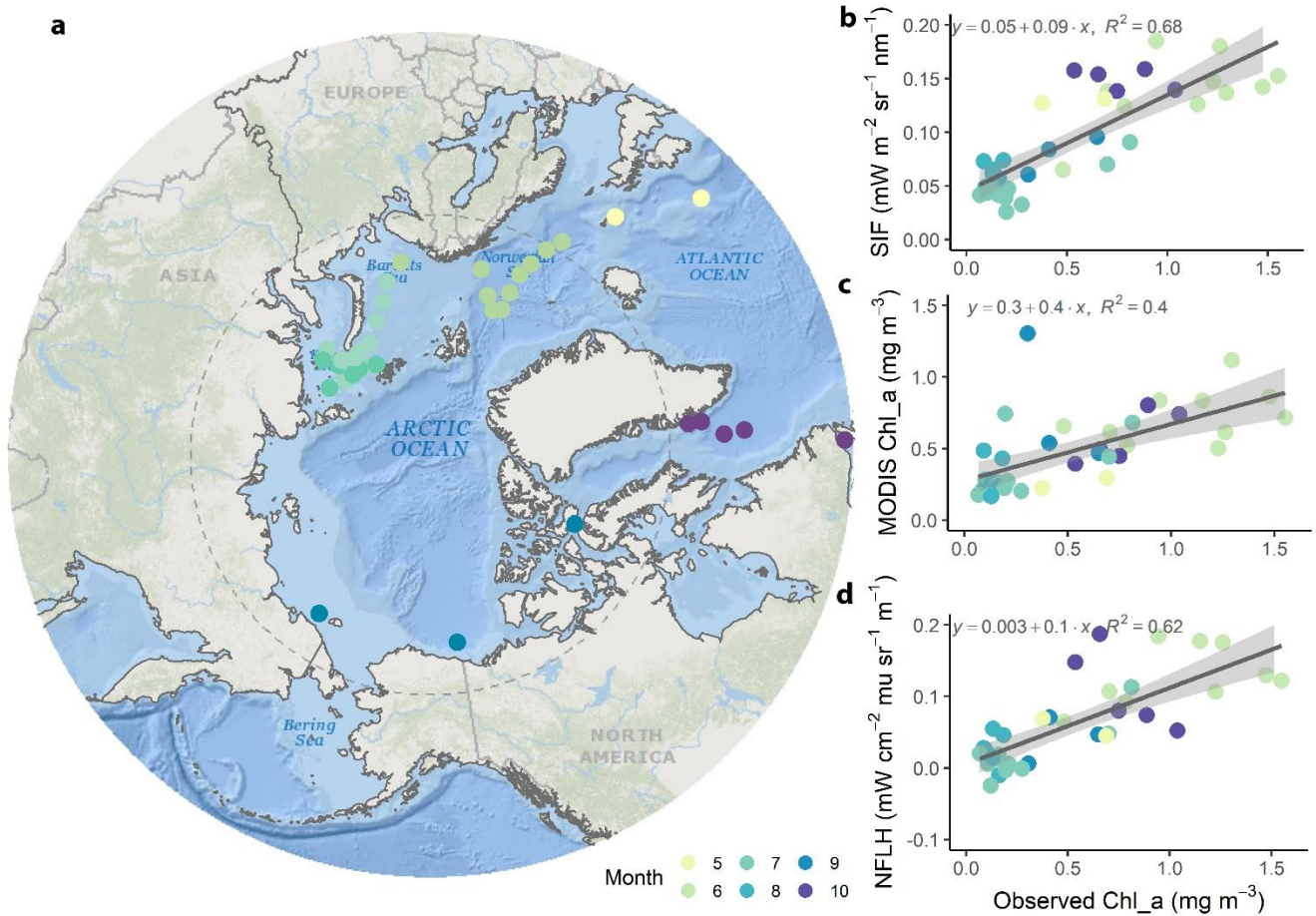


195

196 *Figure 3. Comparison between spatially explicit monthly climatology in Random Forest*  
 197 *predicted SIF relative to the observed SIF over the months of Apr to Sep.*

198 The model results indicate remarkable performance in predicting SIF monthly spatial variability  
 199 relative to observed SIF data (Figure 3). When comparing the seasonality of observed and  
 200 predicted SIF over temperature and polar regions, results demonstrate strong and close  
 201 relationships at regional scales (Figure S4). The performance of the predicted SIF became  
 202 evident when compared with MODIS Chl\_a and NFLH, in conjunction with in-situ observations  
 203 of Chl\_a concentrations from the Tara Oceans Polar Circle 2013 cruises. It is important to  
 204 highlight that the robust correlations observed between SIF and measured Chl\_a are particularly  
 205 compelling, given that we utilized predicted SIF data for the year 2013, while relying on 2013  
 206 observed MODIS chlorophyll-a and NFLH data (Figure 4). The spatial correlation between

207 predicted SIF and in situ observations were 28% stronger than was indicated by MODIS Chl\_a  
 208 data.

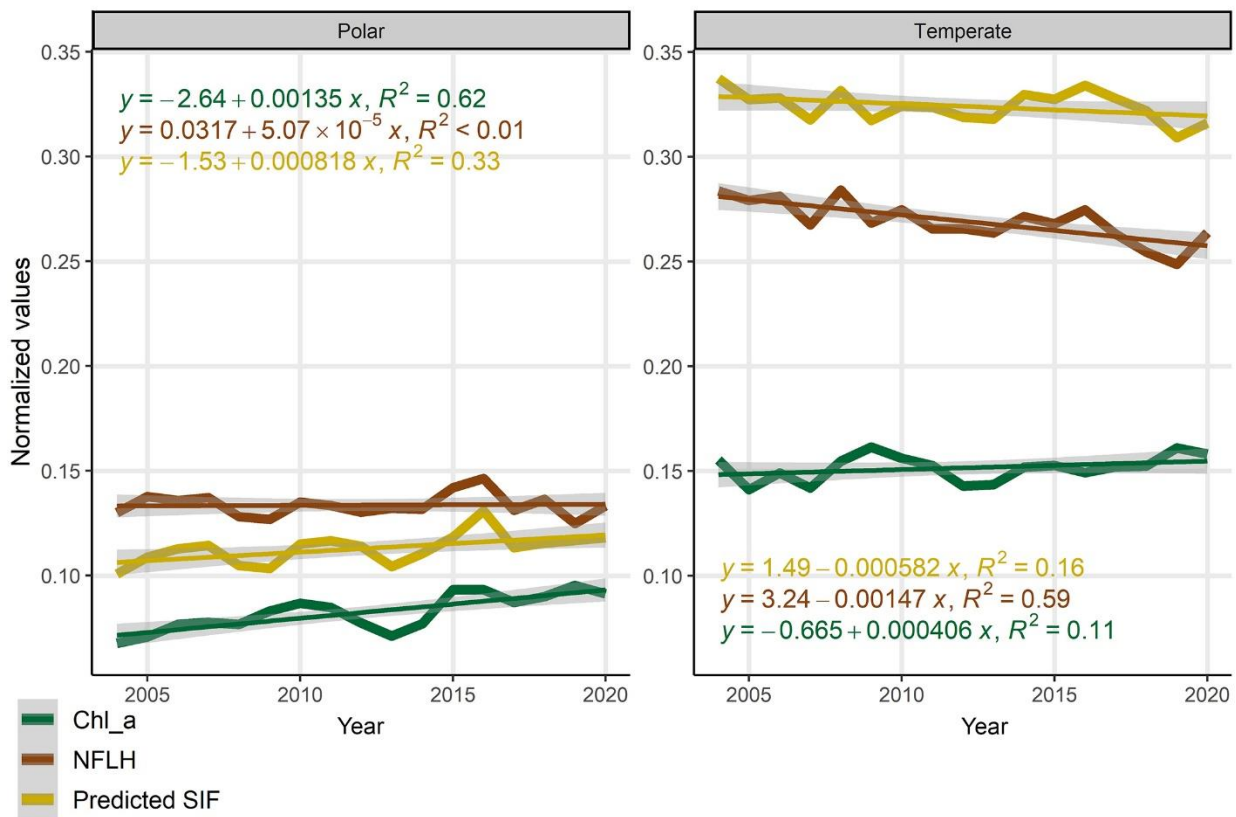


209

210 *Figure 4. Comparison between predicted SIF (2013), Chl\_a and NFLH with HPLC Chl\_a*  
 211 *observations obtained from Tara Oceans Polar Circle 2013 cruises. a location of the retrieved*  
 212 *Chl\_a data from Ocean Circle cruises. b Predicted SIF over 2013 compared to observed Chl\_a. c*  
 213 *MODIS derived Chl\_a over 2013 compared with observed Chl\_a. d MODIS NFLH compared to*  
 214 *observed Chl\_a. Colored dots represent the month of retrieved Chl\_a observations.*

215 We conducted a comparative analysis of trends in MODIS Chl\_a, NFLH, and reconstructed SIF  
 216 across temperate and polar ecoregions (Figure 5). In temperate zones, MODIS Chlor\_a does not  
 217 exhibit a significant trend, but there is a noteworthy decline in NFLH. Conversely, SIF indicates  
 218 a slight decline, particularly evident after 2015, aligning with the observed NFLH trends. In the  
 219 polar regions, Chl\_a exhibits a significant increasing trend, while the NFLH trend is not  
 220 statistically significant. Notably, SIF shows increasing trends, although they are not as  
 221 pronounced as those observed in Chl\_a. The alignment becomes more apparent when examining

222 regional scales and analyzing anomalies in the average SIF over four distinct periods. In this  
 223 context, anomalies were defined as departure from annual means within specified years of data  
 224 records in predicted SIF and NFLH. Notably, differences emerged between SIF and NFLH  
 225 anomalies, particularly from 2008–2011. During this period, predicted SIF exhibited positive  
 226 anomalies over the Kara and Barents seas, in contrast to NFLH (Figure 6). It should be noted that  
 227 unlike NFLH, the RF-predicted SIF is trained on a set of predictive variables that influence  
 228 ocean processes, which can indirectly impact phytoplankton concentration and photochemical  
 229 processes.



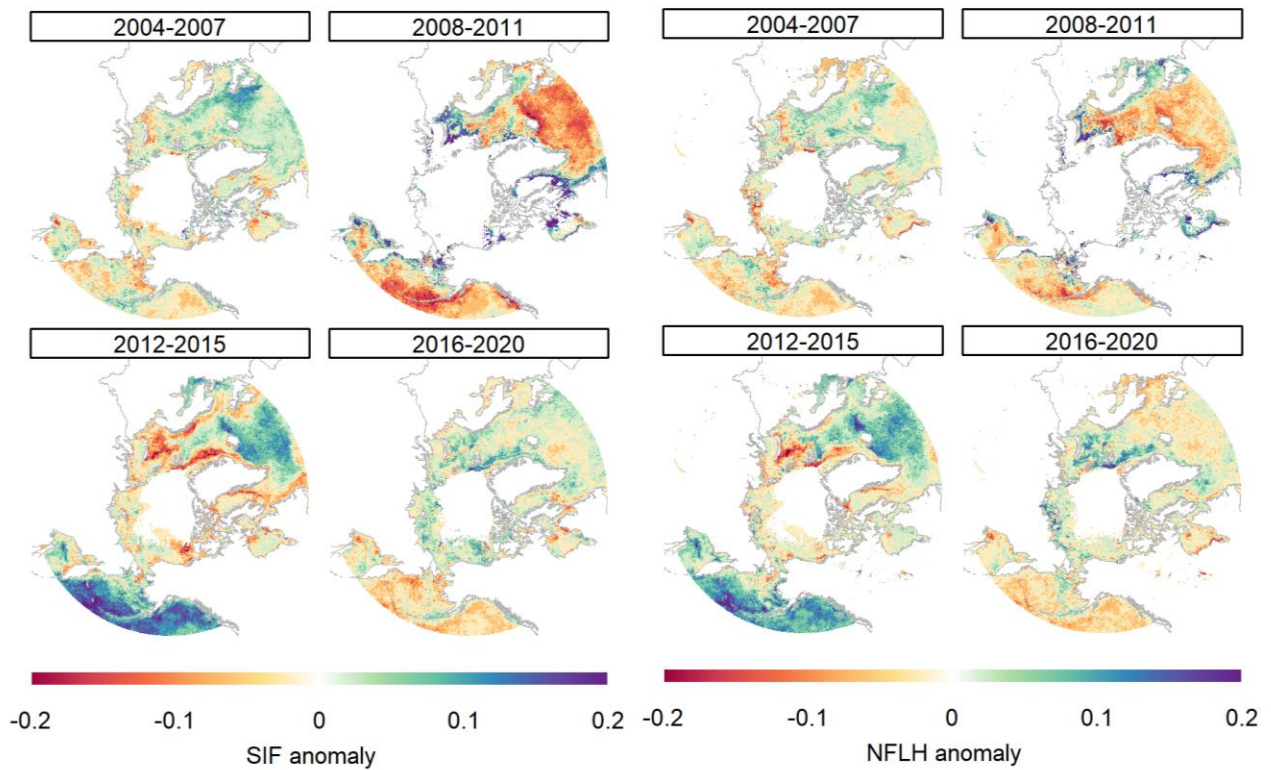
230

231 *Figure 5. Comparison of observed trends in annual Chl\_a, NFLH, and predicted SIF from 2004–*  
 232 *2020. Analysis of the observed trends indicates that the overall trajectory of SIF follows NFLH.*  
 233 *This similarity is especially noticeable in temperate zones, although there are some variations in*  
 234 *specific periods.*

235 However, these disparities in trends and anomalies in SIF concerning Chl\_a and NFLH  
 236 observations underscore the need for cautious utilization of each of these datasets. The observed  
 237 trends and annual variability may not accurately depict the intricacies of ocean photosynthesis

238 process. The representativeness of SIF in capturing the vertical distribution of phytoplankton  
239 remains uncertain at this stage (Köhler *et al* 2020a). Nevertheless, the robust correlations  
240 identified between in situ Chl\_a observations and predicted SIF are highly encouraging. These  
241 findings establish a promising foundation for subsequent analyses and the practical application of  
242 the long-term SIF data generated by this research.

243



244

245 *Figure 6. Comparison of annual-mean anomalies in predicted SIF and observed MODIS NFLH*  
246 *over specific time periods. Anomaly in each period is calculated based on the departure from the*  
247 *2004-2020 means. The analysis of the anomalous data reveals slight regional variations between*  
248 *SIF and NFLH.*

#### 249 **4- Conclusions**

250 We presented a pioneering spatially explicit, long-term SIF dataset over an Arctic Ocean  
251 domain. Our methodology involved utilizing TROPOMI-observed SIF over the ocean, despite its  
252 inherent limitation of a short temporal coverage. To overcome this constraint, we extrapolated  
253 the data to a more extended timeframe by leveraging the relationships among explanatory

254 variables that govern the distribution of phytoplankton. Notably, the TROPOMI SIF data  
255 exhibited a high degree of consistency with MODIS NFLH observations. However, disparities in  
256 long-term trends and anomalies occur, which warrants focused attention in future studies.  
257 Although TROPOMI observations provide the advantage of measuring SIF through optically  
258 thin cloud and aerosol layers, the presence of optically-thick clouds introduces measurement  
259 artifacts (Köhler *et al* 2020a). Furthermore, our predictive modeling approach entails  
260 uncertainties due to the utilization of some predictive variables that are themselves modeled  
261 (ocean state estimates). Nevertheless, this represents the initial step in aiding our comprehension  
262 of long-term changes in Arctic Ocean ecosystems and the influence of ongoing climate change  
263 on ocean productivity and ecosystem dynamics.

## 264 **Acknowledgments**

265 This research was carried out at the Jet Propulsion Laboratory, California Institute of  
266 Technology, under a contract with the National Aeronautics and Space Administration.  
267 Copyright 2024, California Institute of Technology. All rights reserved. Government funding  
268 acknowledged. MM acknowledges financial support from NASA via the Inter Disciplinary  
269 Science Program (IDS19-0113).

## 270 **Open Research**

271 All data used in this research are publicly available from the cited literature and the links below:  
272 MODIS data including Chl\_a and NFLH are available to download from LP DACC data pool:

273 <https://lpdaac.usgs.gov/tools/data-pool/>

274 TROPOMI SIF data are available on Caltech Data repository:

275 <https://data.caltech.edu/records/8hm1f-w5492>

276 ECCO-Darwin model fields are available at:

277 <https://data.nas.nasa.gov/ecco>

278 All analysis were performed in R using open-source software packages:

279 <https://www.R-project.org>

280 R software codes are available on:

281 <https://github.com/MadaniN/Ocean-SIF>

282 Dataset produced by this research are available on ORNL DAAC:

283 Temporary link: [<https://shorturl.at/fqEP1>]

284

285

## 286 **Conflict of Interest**

287 The authors declare no conflicts of interest relevant to this study.

288

## 289 **References**

290  
291 Ardyna M, Babin M, Gosselin M, Devred E, Rainville L and Tremblay J-É 2014 Recent Arctic  
292 Ocean sea ice loss triggers novel fall phytoplankton blooms *Geophys. Res. Lett.* **41** 6207–12

- 293 Arrigo K R and Van Dijken G L 2011 Secular trends in Arctic Ocean net primary production *J.*  
294 *Geophys. Res. Ocean.* **116** 1–15
- 295 Arrigo K R, Matrai P A and Dijken G L Van 2011 Primary productivity in the Arctic Ocean:  
296 Impacts of complex optical properties and subsurface chlorophyll maxima on large scale  
297 estimates *J. Geophys. Res.* **116** 1–15
- 298 Behrenfeld M J and Falkowski P G 1997 Photosynthetic rates derived from satellitebased  
299 chlorophyll concentration *Limnol. Oceanogr.* **41** 1–20
- 300 Behrenfeld M J, Westberry T K, Boss E S, O’Malley R T, Siegel D A, Wiggert J D, Franz B A,  
301 McClain C R, Feldman G C, Doney S C, Moore J K, Dall’Olmo G, Milligan A J, Lima I  
302 and Mahowald N 2009 Satellite-detected fluorescence reveals global physiology of ocean  
303 phytoplankton *Biogeosciences* **6** 779–94
- 304 Bélanger S, Ehn J K and Babin M 2007 Impact of sea ice on the retrieval of water-leaving  
305 reflectance, chlorophyll a concentration and inherent optical properties from satellite ocean  
306 color data *Remote Sens. Environ.* **111** 51–68
- 307 Bouman H A, Jackson T, Sathyendranath S and Platt T 2020 Vertical structure in chlorophyll  
308 profiles: Influence on primary production in the Arctic Ocean: Vertical Structure in Arctic  
309 Chlorophyll *Philos. Trans. R. Soc. A Math. Phys. Eng. Sci.* **378**
- 310 Buitenhuis E T, Hashioka T and Quéré C Le 2013 Combined constraints on global ocean  
311 primary production using observations and models *Global Biogeochem. Cycles* **27** 847–58
- 312 Carroll D, Menemenlis D, Adkins J F, Bowman K W, Brix H, Dutkiewicz S, Fenty I, Gierach M  
313 M, Hill C, Jahn O, Landschützer P, Lauderdale J M, Liu J, Manizza M, Naviaux J D,  
314 Rödenbeck C, Schimel D S, Van der Stocken T and Zhang H 2020 The ECCO-Darwin  
315 Data-Assimilative Global Ocean Biogeochemistry Model: Estimates of Seasonal to  
316 Multidecadal Surface Ocean pCO<sub>2</sub> and Air-Sea CO<sub>2</sub> Flux *J. Adv. Model. Earth Syst.* **12**
- 317 Castagno A P, Wagner T J W, Cape M R, Lester C W, Bailey E, Alves-de-Souza C, York R A  
318 and Fleming A H 2023 Increased sea ice melt as a driver of enhanced Arctic phytoplankton  
319 blooming *Glob. Chang. Biol.* **29** 5087–98
- 320 Core Team R 2017 R: a Language and Environment for Statistical computing
- 321 Cota G F, Harrison W G, Platt T, Sathyendranath S and Stuart V 2003 Bio-optical properties of  
322 the Labrador Sea *J. Geophys. Res. Ocean.* **108**
- 323 Dvoretzky V G, Vodopianova V V. and Bulavina A S 2023 Effects of Climate Change on  
324 Chlorophyll a in the Barents Sea: A Long-Term Assessment *Biology (Basel)*. **12**
- 325 Frankenberg C, Fisher J B, Worden J, Badgley G, Saatchi S S, Lee J E, Toon G C, Butz A, Jung  
326 M, Kuze A and Yokota T 2011 New global observations of the terrestrial carbon cycle from  
327 GOSAT: Patterns of plant fluorescence with gross primary productivity *Geophys. Res. Lett.*  
328 **38** 1–6
- 329 Friedlingstein P, O’Sullivan M, Jones M W, Andrew R M, Bakker D C E, Hauck J, Landschützer  
330 P, Le Quéré C, Luijkx I T, Peters G P, Peters W, Pongratz J, Schwingshackl C, Sitch S,  
331 Canadell J G, Ciais P, Jackson R B, Alin S R, Anthoni P, Barbero L, Bates N R, Becker M,

- 332 Bellouin N, Decharme B, Bopp L, Brasika I B M, Cadule P, Chamberlain M A, Chandra N,  
333 Chau T-T-T, Chevallier F, Chini L P, Cronin M, Dou X, Enyo K, Evans W, Falk S, Feely R  
334 A, Feng L, Ford D J, Gasser T, Ghattas J, Gkritzalis T, Grassi G, Gregor L, Gruber N,  
335 Gürses Ö, Harris I, Hefner M, Heinke J, Houghton R A, Hurtt G C, Iida Y, Ilyina T,  
336 Jacobson A R, Jain A, Jarníková T, Jersild A, Jiang F, Jin Z, Joos F, Kato E, Keeling R F,  
337 Kennedy D, Klein Goldewijk K, Knauer J, Korsbakken J I, Körtzinger A, Lan X, Lefèvre  
338 N, Li H, Liu J, Liu Z, Ma L, Marland G, Mayot N, McGuire P C, McKinley G A, Meyer G,  
339 Morgan E J, Munro D R, Nakaoka S-I, Niwa Y, O'Brien K M, Olsen A, Omar A M, Ono T,  
340 Paulsen M, Pierrot D, Pocock K, Poulter B, Powis C M, Rehder G, Resplandy L, Robertson  
341 E, Rödenbeck C, Rosan T M, Schwinger J, et al 2023 Global Carbon Budget 2023 *Earth*  
342 *Syst. Sci. Data* **15** 5301–69
- 343 Genuer R, Poggi J M and Tuleau-Malot C 2010 Variable selection using random forests *Pattern*  
344 *Recognit. Lett.* **31** 2225–36 Online: <http://dx.doi.org/10.1016/j.patrec.2010.03.014>
- 345 Gorelick N, Hancher M, Dixon M, Ilyushchenko S, Thau D and Moore R 2017 Google Earth  
346 Engine: Planetary-scale geospatial analysis for everyone *Remote Sens. Environ.* **202** 18–27
- 347 Guanter L, Zhang Y, Jung M, Joiner J, Voigt M, Berry J a., Frankenberg C, Huete A R, Zarco-  
348 Tejada P, Lee J-E J-E, Moran M S, Ponce-Campos G, Beer C, Camps-Valls G, Buchmann  
349 N, Gianelle D, Klumpp K, Cescatti A, Baker J M and Griffis T J 2014 Global and time-  
350 resolved monitoring of crop photosynthesis with chlorophyll fluorescence *Proc. Natl. Acad.*  
351 *Sci.* **111** E1327-33 Online: <http://www.ncbi.nlm.nih.gov/pubmed/24706867>
- 352 Guidi L, Ras J, Claustre H, Pesant S, Tara Oceans Consortium C and Tara Oceans Expedition P  
353 2017 Environmental context of all samples from the Tara Oceans Expedition (2009-2013),  
354 about pigment concentrations (HPLC) in the targeted environmental feature *Tara Ocean.*  
355 *Consortium, Coord. Tara Ocean. Exped. Particip. Regist. all samples from Tara Ocean.*  
356 *Exped. (2009-2013). PANGAEA, <https://doi.org/10.1594/PANGAEA.875582> Online:*  
357 <https://doi.org/10.1594/PANGAEA.875569>
- 358 Gupana R S, Odermatt D, Cesana I, Giardino C, Nedbal L and Damm A 2021 Remote sensing of  
359 sun-induced chlorophyll-a fluorescence in inland and coastal waters: Current state and  
360 future prospects *Remote Sens. Environ.* **262** 112482 Online:  
361 <https://doi.org/10.1016/j.rse.2021.112482>
- 362 Hu C, Feng L, Lee Z, Franz B A, Bailey S W, Werdell P J and Proctor C W 2019 Improving  
363 Satellite Global Chlorophyll a Data Products Through Algorithm Refinement and Data  
364 Recovery *J. Geophys. Res. Ocean.* **124** 1524–43
- 365 Hu C, Lee Z and Franz B 2012 Chlorophyll a algorithms for oligotrophic oceans: A novel  
366 approach based on three-band reflectance difference *J. Geophys. Res. Ocean.* **117** 1–25
- 367 Jiao W, Chang Q and Wang L 2019 The Sensitivity of Satellite Solar-Induced Chlorophyll  
368 Fluorescence to Meteorological Drought *Earth's Futur.* **7** 558–73
- 369 Johnson K S and Bif M B 2021 Constraint on net primary productivity of the global ocean by  
370 Argo oxygen measurements *Nat. Geosci.* **14** 769–74 Online:  
371 <http://dx.doi.org/10.1038/s41561-021-00807-z>
- 372 Jung M, Reichstein M, Margolis H A, Cescatti A, Richardson A D, Arain M A, Arneth A,

- 373 Bernhofer C, Bonal D, Chen J, Gianelle D, Gobron N, Kiely G, Kutsch W, Lasslop G, Law  
374 B E, Lindroth A, Merbold L, Montagnani L, Moors E J, Papale D, Sottocornola M, Vaccari  
375 F and Williams C 2011 Global patterns of land - atmosphere fluxes of carbon dioxide ,  
376 latent heat , and sensible heat derived from eddy covariance , satellite , and meteorological  
377 observations **116** 1–16
- 378 Kim J E, Wang J A, Li Y, Czimczik C I and Randerson J T 2024 Wildfire-induced increases in  
379 photosynthesis in boreal forest ecosystems of North America *Glob. Chang. Biol.* **30**
- 380 Ko E, Gorbunov M Y, Jung J, Lee Y, Cho K H, Yang E J and Park J 2022 Phytoplankton  
381 photophysiology varies depending on nitrogen and light availability at the subsurface  
382 chlorophyll maximum in the northern Chukchi Sea *Front. Mar. Sci.* **9** 1–18
- 383 Köhler P, , Michael J. Behrenfeld , Jochen Landgraf, Troy S. Magney C F, Behrenfeld M J,  
384 Landgraf J, Joiner J, Magney T S, Frankenberg C, Köehler P, Frankenberg C, Magney T S,  
385 Guanter L, Joiner J, Landgraf J and Köhler, P., Behrenfeld, M. J., Landgraf, J., Joiner, J.,  
386 Magney, T. S., & Frankenberg C 2020a Global Retrievals of Solar-Induced Chlorophyll  
387 Fluorescence at Red Wavelengths With TROPOMI *Geophys. Res. Lett.* **47** 456–63 Online:  
388 <http://doi.wiley.com/10.1029/2018GL079031>
- 389 Köhler P, Behrenfeld M J, Landgraf J, Joiner J, Magney T S and Frankenberg C 2020b Global  
390 Retrievals of Solar-Induced Chlorophyll Fluorescence With TROPOMI
- 391 Köhler P, Frankenberg C, Magney T S, Guanter L, Joiner J and Landgraf J 2018 Global  
392 Retrievals of Solar-Induced Chlorophyll Fluorescence With TROPOMI: First Results and  
393 Intersensor Comparison to OCO-2 *Geophys. Res. Lett.* **45** 10,456-10,463
- 394 Lee Y J, Matrai P A, Friedrichs M A M, Saba V S, Antoine D, Ardyna M, Asanuma I, Babin M,  
395 Bélanger S, Benoît-Gagné M, Devred E, Fernández-Méndez M, Gentili B, Hirawake T,  
396 Kang S H, Kameda T, Katlein C, Lee S H, Lee Z, Mélin F, Scardi M, Smyth T J, Tang S,  
397 Turpie K R, Waters K J and Westberry T K 2015 An assessment of phytoplankton primary  
398 productivity in the Arctic Ocean from satellite ocean color/in situ chlorophyll-a based  
399 models *J. Geophys. Res. Ocean.* **120** 6508–41
- 400 Lewis K M, Van Dijken G L and Arrigo K R 2020 Changes in phytoplankton concentration now  
401 drive increased Arctic Ocean primary production *Science (80-. )*. **369** 198–202
- 402 Li J, Matsuoka A, Hooker S B, Maritorea S, Pang X and Babin M 2023 A tuned ocean color  
403 algorithm for the Arctic Ocean: a solution for waters with high CDM content *Opt. Express*  
404 **31** 38494
- 405 Li X and Xiao J 2019 A global, 0.05-degree product of solar-induced chlorophyll fluorescence  
406 derived from OCO-2, MODIS, and reanalysis data *Remote Sens.* **11**
- 407 Liaw A and Wiener M 2002 Classification and Regression by randomForest *R News* **2** 18–22
- 408 Liu J, Wennberg P O, Parazoo N C, Yin Y and Frankenberg C 2020 Observational Constraints  
409 on the Response of High-Latitude Northern Forests to Warming *AGU Adv.* **1**
- 410 Madani N, Kimball J S, Ballantyne A P, Affleck D L R, Van Bodegom P M, Reich P B, Kattge  
411 J, Sala A, Nazeri M, Jones M O, Zhao M and Running S W 2018 Future global productivity  
412 will be affected by plant trait response to climate *Sci. Rep.* **8**

- 413 Madani N, Parazoo N C, Kimball J S, Reichle R H, Chatterjee A, Watts J D, Saatchi S, Liu Z,  
414 Endsley A, Tagesson T, Rogers B M, Xu L, Wang J A, Magney T and Miller C E 2021 The  
415 Impacts of Climate and Wildfire on Ecosystem Gross Primary Productivity in Alaska *J.*  
416 *Geophys. Res. Biogeosciences* **126** 1–14
- 417 Madani N, Parazoo N C and Miller C E 2023 Climate change is enforcing physiological changes  
418 in Arctic Ecosystems *Environ. Res. Lett.* **18** 074027
- 419 Magney T S, Bowling D R, Logan B A, Grossmann K, Stutz J, Blanken P D, Burns S P, Cheng  
420 R, Garcia M A, Köhler P, Lopez S, Parazoo N C, Raczka B, Schimel D and Frankenberg C  
421 2019 Mechanistic evidence for tracking the seasonality of photosynthesis with solar-  
422 induced fluorescence *Proc. Natl. Acad. Sci. U. S. A.* **116** 11640–5
- 423 Manizza M, Carroll D, Menemenlis D, Zhang H and Miller C E 2023 Modeling the Recent  
424 Changes of Phytoplankton Blooms Dynamics in the Arctic Ocean *J. Geophys. Res. Ocean.*  
425 **128**
- 426 Matsuoka A, Boss E, Babin M, Karp-Boss L, Hafez M, Chekalyuk A, Proctor C W, Werdell P J  
427 and Bricaud A 2017 Pan-Arctic optical characteristics of colored dissolved organic matter:  
428 Tracing dissolved organic carbon in changing Arctic waters using satellite ocean color data  
429 *Remote Sens. Environ.* **200** 89–101 Online: <http://dx.doi.org/10.1016/j.rse.2017.08.009>
- 430 Mohammadi K, Jiang Y and Wang G 2022 Flash drought early warning based on the trajectory  
431 of solar-induced chlorophyll fluorescence *Proc. Natl. Acad. Sci. U. S. A.* **119** 1–9
- 432 NASA 2014 MODIS-Aqua Ocean Color Data *NASA Goddard Sp. Flight Centre, Ocean Ecol.*  
433 *Lab. Ocean Biol. Process. Gr.*
- 434 Natali S M, Watts J D, Rogers B M, Potter S, Ludwig S M, Selbmann A K, Sullivan P F, Abbott  
435 B W, Arndt K A, Birch L, Björkman M P, Bloom A A, Celis G, Christensen T R,  
436 Christiansen C T, Commane R, Cooper E J, Crill P, Czimczik C, Davydov S, Du J, Egan J  
437 E, Elberling B, Euskirchen E S, Friborg T, Genet H, Göckede M, Goodrich J P, Grogan P,  
438 Helbig M, Jafarov E E, Jastrow J D, Kalhori A A M, Kim Y, Kimball J S, Kutzbach L, Lara  
439 M J, Larsen K S, Lee B Y, Liu Z, Loranty M M, Lund M, Lupascu M, Madani N, Malhotra  
440 A, Matamala R, McFarland J, McGuire A D, Michelsen A, Minions C, Oechel W C,  
441 Olefeldt D, Parmentier F J W, Pirk N, Poulter B, Quinton W, Rezanezhad F, Risk D, Sachs  
442 T, Schaefer K, Schmidt N M, Schuur E A G, Semenchuk P R, Shaver G, Sonnentag O, Starr  
443 G, Treat C C, Waldrop M P, Wang Y, Welker J, Wille C, Xu X, Zhang Z, Zhuang Q and  
444 Zona D 2019 Large loss of CO<sub>2</sub> in winter observed across the northern permafrost region  
445 *Nat. Clim. Chang.* **9** 852–7
- 446 Parazoo N C, Bowman K, Fisher J B, Frankenberg C, Jones D B A, Cescatti A, Pérez-Priego Ó,  
447 Wohlfahrt G and Montagnani L 2014 Terrestrial gross primary production inferred from  
448 satellite fluorescence and vegetation models *Glob. Chang. Biol.* **20** 3103–21
- 449 Parazoo N C, Frankenberg C, Köhler P, Joiner J, Yoshida Y, Magney T, Sun Y and Yadav V  
450 2019 Towards a Harmonized Long-Term Spaceborne Record of Far-Red Solar-Induced  
451 Fluorescence *J. Geophys. Res. Biogeosciences*
- 452 Silsbe G M, Behrenfeld M J, Halsey K H, Milligan A J and Westberry T K 2016 The CAFE  
453 model: A net production model for global ocean phytoplankton *Global Biogeochem. Cycles*

454           **30** 1756–77

455       Singh A, Fietz S, Thomalla S J, Sanchez N, Ardelan M V., Moreau S, Kauko H M, Fransson A,  
456           Chierici M, Samanta S, Mtshali T N, Roychoudhury A N and Ryan-Keogh T J 2023  
457           Absence of photophysiological response to iron addition in autumn phytoplankton in the  
458           Antarctic sea-ice zone *Biogeosciences* **20** 3073–91

459       Spalding M D, Fox H E, Allen G R, Davidson N, Ferdaña Z A, Finlayson M, Halpern B S, Jorge  
460           M A, Lombana A, Lourie S A, Martin K D, McManus E, Molnar J, Recchia C A and  
461           Robertson J 2007 Marine ecoregions of the world: A bioregionalization of coastal and shelf  
462           areas *Bioscience* **57** 573–83

463       Westberry T, Behrenfeld M J, Siegel D A and Boss E 2008 Carbon-based primary productivity  
464           modeling with vertically resolved photoacclimation *Global Biogeochem. Cycles* **22** 1–18

465       Zhang Y, Joiner J, Alemohammad S H, Zhou S and Gentine P 2018 A global spatially  
466           contiguous solar-induced fluorescence (CSIF) dataset using neural networks *Biogeosciences*  
467           **15** 5779–800 Online: <https://www.biogeosciences.net/15/5779/2018/>

468       Zhao H, Matsuoka A, Manizza M and Winter A 2022 Recent Changes of Phytoplankton Bloom  
469           Phenology in the Northern High-Latitude Oceans (2003–2020) *J. Geophys. Res. Ocean.* **127**

470

471